Article | Open Access

Energy Materials

Wu *et al. Energy Mater.* **2026**, *6*, 600054 **DOI:**10.20517/energymater.2026.10

High energy density and efficiency in all-organic P(VDF-TrFE-CFE)/PMMA dielectric films enabled by dipolar interaction and γ-irradiation

Yabo Wu[1,#], Zhiqiang Zhang[1,#], Yihao Zhang[3,#], Zhaoxin Ma[1,#], Changji Deng[1], Song Zhang[1], Bowen Bai[2], Weicong Liu[2], Yifan Huang[2,*], Qingfeng Zhang[1,*], Yongming Hu[1,*]

Keywords:
P(VDF-TrFE-CFE)/PMMA, dipolar interaction, γ-irradiation, dielectric energy storage, energy density and efficiency

Citation: Wu, Y.; Zhang, Z.; Zhang, Y.; Ma, Z.; Deng, C.; Zhang, S.; Bai, B.; Liu, W.; Huang, Y.; Zhang, Q.; Hu, Y. High energy density and efficiency in all-organic P(VDF-TrFE-CFE)/PMMA dielectric films enabled by dipolar interaction and γ-irradiation. *Energy Mater.* **2026**, *6*, 600054. https://dx.doi.org/10.20517/energymater.2026.10

Received: 24 Jan 2026 **First Decision:** 28 Feb 2026 **Revised:** 20 Mar 2026 **Accepted:** 30 Apr 2026 **Published:** 25 May 2026

Academic Editor: Soo Young Kim **Copy Editor:** Ping Zhang **Production Editor:** Ping Zhang

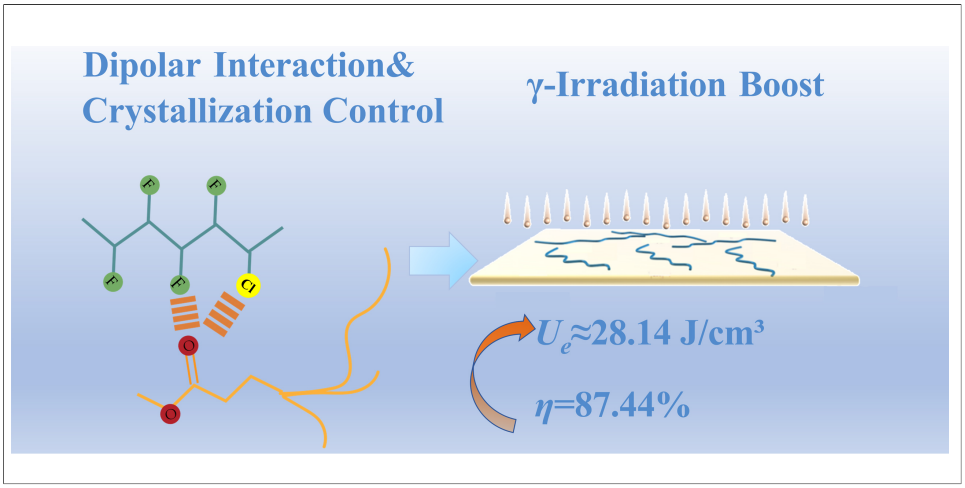

Abstract

Polymer dielectrics are promising materials for electrostatic capacitors because of their high dielectric strength and fast charge-discharge capability. However, improving the energy-storage density of fluorinated ferroelectric polymers remains challenging because enhanced polarization is often accompanied by reduced breakdown strength. In this work, all-organic poly(vinylidene fluoride- trifluoroethylene-chlorofluoroethylene)/poly(methyl methacrylate) [P(VDF-TrFE-CFE)/PMMA] dielectric films are prepared by solution blending and casting. By tuning the blend ratio, the intermolecular interactions and crystallization behavior of the films are systematically regulated, resulting in distinct changes in their electrical properties. The results suggest that dipolar interactions between PMMA carbonyl groups and polar groups in P(VDF-TrFE-CFE) disturb chain packing and suppress crystallization, thereby reducing dielectric loss and improving breakdown stability. At the optimized composition, the P(VDF-TrFE-CFE)/PMMA (50/50 wt.%) film

[1]Hubei Key Laboratory of Micro-Nanoelectronic Materials and Devices, Hubei University, Wuhan 430062, Hubei, China.
[2]Research Institute of Physical Sciences in Special Environments, Harbin Institute of Technology (Shenzhen), Shenzhen 518055, Guangdong, China.
[3]College of Energy Materials and Chemistry, Inner Mongolia University, Hohhot, 010021, Inner Mongolia, China.
[#]Authors contributed equally.

[*]**Correspondence to:** Prof. Yifan Huang, Research Institute of Physical Sciences in Special Environments, Harbin Institute of Technology (Shenzhen), Shenzhen 518055, Guangdong, China. E-mail: yifanhuang@hit.edu.cn; Prof. Qingfeng Zhang, Prof. Yongming Hu, Hubei Key Laboratory of Micro-Nanoelectronic Materials and Devices, Hubei University, Wuhan 430062, Hubei, China. E-mail: zhangqingfeng@hubu.edu.cn; huym@hubu.edu.cn

delivers a dischaged energy density of 17.12 J/cm^3 with an energy-storage efficiency of 88.11%. Further γ-irradiation of the optimized film at doses of 10-150 kGy leads to additional improvement in dielectric energy-storage performance. These results demonstrate that regulating intermolecular interactions and crystalline morphology through all-organic blending and irradiation is an effective strategy for developing high-performance polymer dielectrics.

INTRODUCTION

With the rapid development of high-power electronic devices, pulsed-power systems, and advanced power-electronic technologies, dielectric capacitors are facing increasingly stringent requirements in terms of high energy density, high charge-discharge efficiency, and long-term operational reliability[1-5]. Polymeric dielectrics play an important role in electrostatic energy storage because of their high dielectric strength, low loss, fast switching characteristics, and good processability. However, the commercial standard, biaxially oriented polypropylene (BOPP), is strictly limited by its insufficient dielectric constant. Because of this, the stored energy density within these linear polymers generally saturates under 2-3 J/cm^3, which falls short of the rigorous demands for compact and high-integration electronic systems[6,7].

Poly (vinylidene fluoride) (PVDF)-based relaxor ferroelectric polymers exhibit high dielectric constant and strong polarization, mainly because the highly polar C-F bonds provide large dipole moments along the polymer chains, giving these materials considerable potential for high-energy-density energy storage[8,9]. However, PVDF-based materials typically contain large ferroelectric domains and pronounced crystalline structures, which tend to result in high remanent polarization and dielectric loss. Meanwhile, conduction loss and local electric-field concentration effects can significantly reduce the breakdown strength, thereby constraining the simultaneous improvement of discharged energy density and charge-discharge efficiency[10,11]. Therefore, achieving a balance between maintaining high effective polarization while suppressing remanent polarization and charge-carrier transport has become a central challenge in the design of PVDF-based dielectric energy-storage materials.

In recent years, all-organic polymer blending has been regarded as an effective strategy that balances property regulation with processing feasibility. Previous studies have shown that introducing linear polymers into PVDF-based systems can, to some extent, suppress the growth of ferroelectric domains, reduce remanent polarization, and enhance breakdown strength[12,13]. For example, Han *et al.* achieved uniform dispersion of polypropylene (PP) in PP/PVDF blends by regulating the phase structure and crystallization kinetics during processing, and further constructed a sandwich architecture to mitigate hysteresis loss. The resulting film delivered a discharged energy density of 8.1 J/cm^3 and an energy-storage efficiency of 75%, indicating that the introduction of a small amount of a nonpolar phase can improve discharge efficiency without markedly sacrificing polarization[14]. Luo *et al.* prepared poly(vinylidene fluoride-trifluoroethylene-chlorofluoroethylene)/poly(methyl methacrylate) [P(VDF-TrFE-CFE)/PMMA] films by blending and thermoforming, and obtained a discharged energy density of 11.2 J/cm^3 with an efficiency of 85.8% at 4,750 kV/cm. Their results suggested that interfacial interactions, chain entanglement, and phase morphology play important roles in narrowing the polarization-electric field (*P-E*) loops and improving performance[15]. Nevertheless, most existing studies have focused on macroscopic performance optimization. A systematic understanding of molecular-scale dipolar interactions, crystallinity evolution, and their coupled effects on energy-storage behavior is still lacking, especially in relaxor ferroelectric polymer systems.

To elucidate the relationship between microstructural features and macroscopic energy-storage performance in all-organic polymer blends, poly(vinylidene fluoride-trifluoroethylene-chlorofluoroethylene) [P(VDF-TrFE-CFE)] is used as the relaxor-ferroelectric matrix. PMMA, which possesses good

insulation capability and chemical stability, is introduced as a modifying component to construct P(VDF-TrFE-CFE)/PMMA blend films. By tuning the PMMA content, we systematically investigate its influence on crystallization behavior and energy-storage properties. At a P(VDF-TrFE-CFE)/PMMA mass ratio of 50/50, the blend achieves a discharged energy density of 17.12 J/cm^3 and an energy-storage efficiency of 88.11%, corresponding to increases of 53.9% and 64.2%, respectively, compared with pristine P(VDF-TrFE-CFE). In addition, the optimized film is subjected to γ-irradiation at different doses (10-150 kGy) to further explore the energy-storage potential of this system. Taken together, these results provide a useful structure-property framework based on molecular dipolar interactions and crystallinity regulation for the development of high-energy-density and high-efficiency all-organic dielectrics.

EXPERIMENT

Materials

P(VDF-TrFE-CFE) (64.8/27.4/7.8 mol%) (ARKEMA 64-019, France) was purchased from Chaogan Technology (Beijing) Co., Ltd. PMMA was provided by Sigma Aldrich. N, N-Dimethylformamide (DMF, 99.9%, Aladdin) was used as a solvent. All materials and reagents were used as received without any additional purification.

Fabrication of copolymeric blend films

P(VDF-TrFE-CFE) and PMMA powders were weighed at mass ratios of 0/100, 40/60, 50/50, 70/30, and 100/0 and dissolved in DMF to obtain solutions with a concentration of 0.1 g/mL. The solutions were stirred at 40 °C for 12 h until transparent and homogeneous. Each precursor solution was cast onto a quartz glass substrate and leveled with a doctor blade to ensure uniform film thickness. The resulting films were dried in a vacuum oven at 70 °C and 0.08 MPa for 12 h, followed by thermal treatment at 130 °C for 10 min. The glass substrates were then immersed in deionized water to peel off the films. After complete drying, the films were used for subsequent characterization. The film thickness was approximately 12 μm.

Properties characterization

Fourier transform infrared (FTIR) spectra were recorded using a VERTEX 70v spectrometer (Bruker, Germany). Small-angle X-ray scattering (SAXS) measurements were performed on a Xeuss 2.0 system (XENOCS, France). Wide-Angle X-ray Scattering (WAXS) measurements were performed on a Xeuss 3.0 HR (XENOCS, France). X-ray diffraction (XRD) patterns were collected using a D8 Advance diffractometer (Bruker, Germany). Cross-sectional morphologies were examined by field-emission scanning electron microscopy (FE-SEM, SIGMA 500; Zeiss, Germany). Surface topography was characterized by atomic force microscopy (AFM, Dimension Edge; Bruker, Germany). Young's modulus was measured using a universal testing machine (C43.104EY, MTS, USA). Differential scanning calorimetry (DSC) was carried out on a DSC3 instrument (Mettler Toledo, Switzerland). Breakdown strength was evaluated using a withstand voltage tester (NJC5010, Tongguo Technology, China). Ferroelectric hysteresis and leakage current characteristics were measured using a Precision LC II ferroelectric test system (Radiant, USA).

RESULTS AND DISCUSSION

Figure 1 schematically illustrates the design concept of the P(VDF-TrFE-CFE)/PMMA blend films and the expected molecular-level interaction between the two components. The introduction of PMMA is expected to generate dipole-dipole interactions between the two components, which may affect chain packing, segmental mobility, crystallization behavior, and carrier transport in the blend films. Guided by this structural design, the following discussion examines the corresponding structural and electrical evolutions of the blend films through the relevant characterizations and correlates them with their dielectric, breakdown, and energy-storage behaviors.

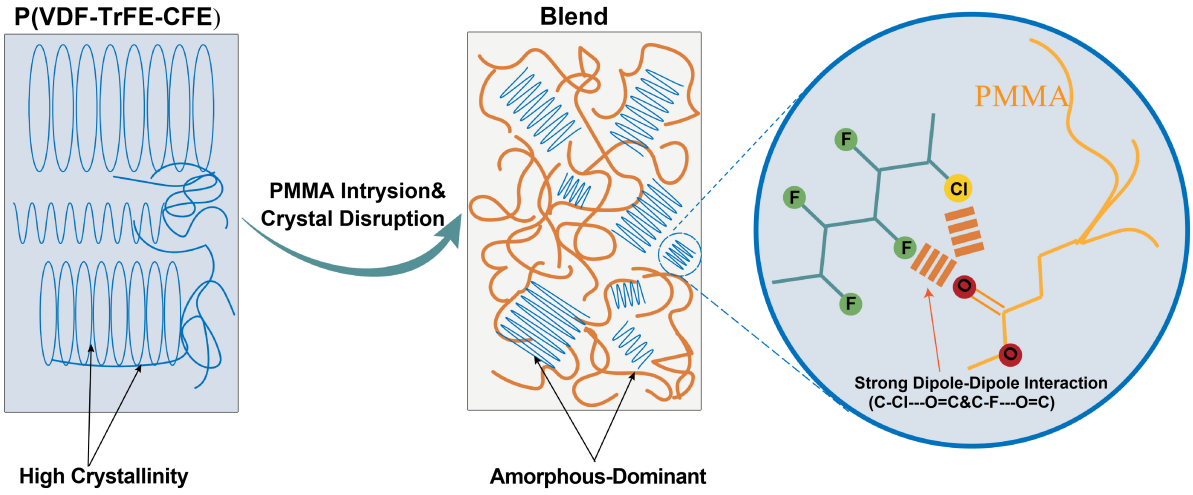

Figure 1. Schematic illustration of the blending-induced structural disordering and interfacial dipole-dipole coupling mechanism in P(VDF-TrFE-CFE)/PMMA films. P(VDF-TrFE-CFE): Poly(vinylidene fluoride- trifluoroethylene-chlorofluoroethylene); PMMA: poly(methyl methacrylate).

Figure 2A shows the XRD profiles of neat P(VDF-TrFE-CFE), neat PMMA, and the blend films. The diffraction envelopes of the blend films progressively evolve from the neat P(VDF-TrFE-CFE) profile toward the broad amorphous halo of neat PMMA with increasing PMMA content. Since PMMA is an amorphous polymer, its incorporation drives the blend films toward a more amorphous-dominant structural state, leading to broader and more diffuse scattering features. At the same time, residual contributions associated with P(VDF-TrFE-CFE)-related ordering are still retained in the blend films. Therefore, the XRD evolution should not be interpreted as a simple shift of a single crystalline reflection. Instead, it reflects the combined effects of the increasing amorphous PMMA character and the suppression of residual P(VDF-TrFE-CFE) ordering[15-19]. To further examine the internal structural evolution, both SAXS and WAXS analyses are performed [Figure 2B-F, Supplementary Figures 1 and 2]. No distinguishable scattering peak is observed in the SAXS profiles. The 2D SAXS patterns show diffuse scattering that attenuates radially from the center, indicating that PMMA blending does not induce a new periodic long-range ordered phase. The WAXS results show clear composition-dependent changes [Figure 2C-F and Supplementary Figure 2]. Compared with neat P(VDF-TrFE-CFE), the blend samples exhibit broader and more diffuse scattering characteristics. In particular, the 50/50 wt.% film shows a broader and more isotropic scattering ring in the 2D WAXS pattern [Figure 2E], indicating a more diffuse scattering distribution rather than a concentrated crystalline feature. Although its corresponding 1D profile in Figure 2C appears relatively strong, this should not be interpreted as a sharper crystalline reflection[20,21]. Instead, it is better understood as a broadened scattering envelope that shifts away from the concentrated terpolymer-dominated feature toward a more amorphous character after blending. With further increasing PMMA content, the scattering feature becomes even more diffuse and gradually approaches the amorphous PMMA-like halo. Overall, the WAXS results indicate progressive broadening and redistribution of scattering with increasing PMMA content, consistent with suppressed crystallization and reduced short-range ordering in the films. The full-range FTIR spectra [Figure 2G] and the enlarged carbonyl (C=O) region [Figure 2H] show that, after blending, the characteristic carbonyl absorption band of PMMA shifts from ~1,724 cm^{-1} in pristine PMMA to ~1,726 cm^{-1} in the blend films, indicating that the local chemical environment of the carbonyl groups is altered after blending. In addition to this change, the absorption envelope in the 1,200-1,100 cm^{-1} region also evolves significantly after blending, with the main band changing from ~1,174 cm^{-1} in pristine P(VDF-TrFE-CFE) to ~1,149-1,144 cm^{-1} in the blend films. Because this region contains overlapping contributions from PMMA and P(VDF-TrFE-CFE), the spectral evolution is more reasonably attributed to changes in the local

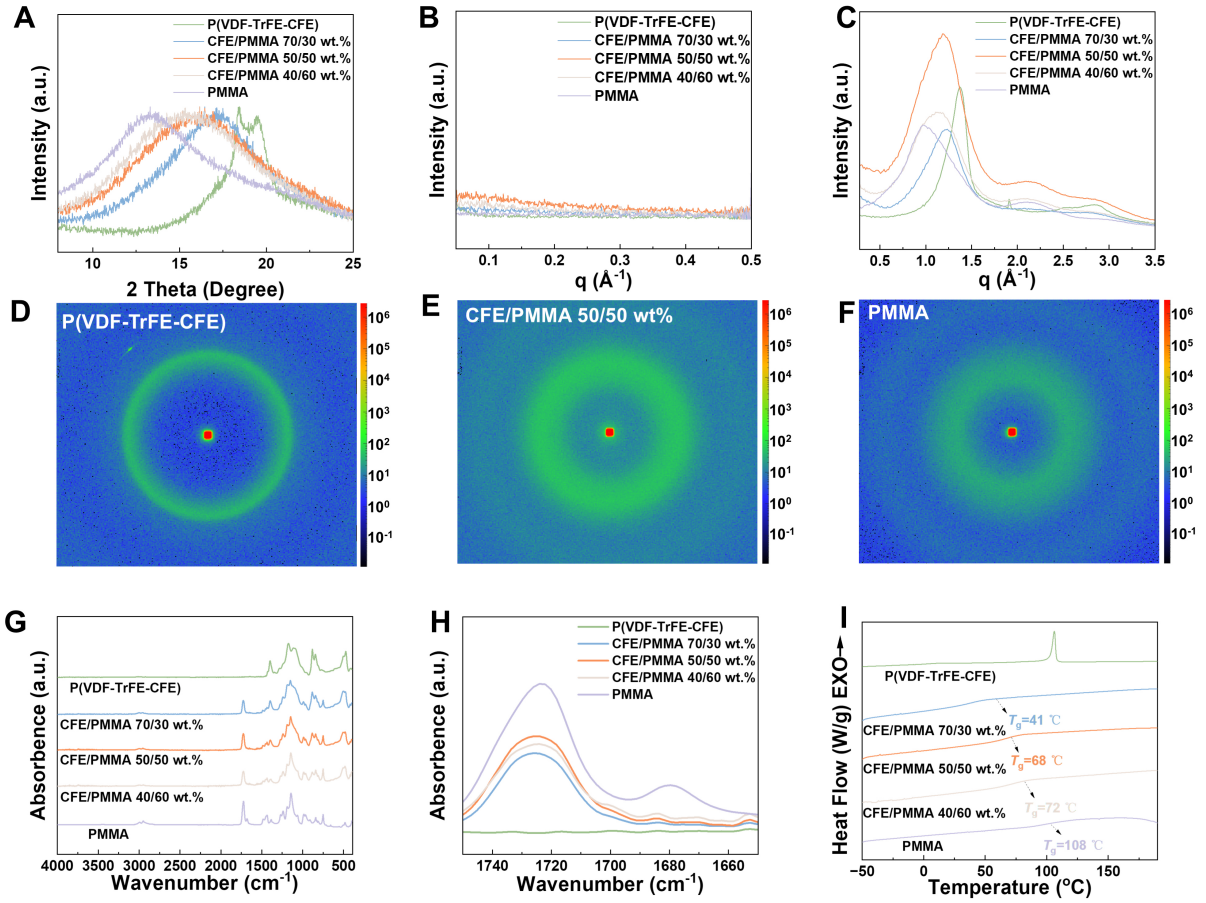

Figure 2. Structural organization, intermolecular interactions, and thermal behavior of P(VDF-TrFE-CFE)/PMMA blend films. (A) XRD patterns of films with different compositions; (B) 1D SAXS profiles; (C) 1D WAXS profiles; 2D WAXS patterns of (D) P(VDF-TrFE-CFE) (E) P(VDF-TrFE-CFE)/PMMA 50/50 wt.%, and (F) PMMA, respectively; (G) FTIR spectra; (H) enlarged FTIR region of the carbonyl band; (I) DSC curves. XRD: X-ray diffraction; SAXS: small-angle X-ray scattering; WAXS: wide-angle X-ray scattering; FTIR: Fourier transform infrared; DSC: differential scanning calorimetry; P(VDF-TrFE-CFE): poly(vinylidene fluoride- trifluoroethylene-chlorofluoroethylene); PMMA: poly(methyl methacrylate); CFE: abbreviation of P(VDF-TrFE-CFE).

environments of both components rather than to the shift of a single assigned bond. Meanwhile, the low-wavenumber fluoropolymer-related bands in the ~900-500 cm^{-1} region remain detectable, but also exhibit correlated changes in peak position and/or relative intensity after blending. This result further indicates that the local chain environments are affected by blending. Taken together, these FTIR results suggest that blending does not simply produce a physical superposition of the two components, but instead changes their local chemical environments. DSC is further employed to examine the thermodynamic features associated with crystallization [Figure 2I]. The pristine P(VDF-TrFE-CFE) film displays a pronounced endothermic melting peak, whereas none of the blend films shows such a melting endotherm; instead, only a single glass-transition temperature (T_g) is observed. Moreover, T_g shifts to higher temperatures with increasing PMMA content, indicating segmental mobility is progressively restricted. These results corroborate that crystallization is effectively suppressed and that the blends are predominantly amorphous[22]. Meanwhile, the presence of a single T_g also supports the overall homogeneity of the blend system from a thermodynamic perspective[23].

To better understand how the PMMA content influences the microstructure of the blend films, cross-sectional SEM and AFM characterizations are further performed on samples with different compositions [Supplementary Figures 3 and 4] to evaluate film continuity, compactness, and surface micro-morphology. The cross-sectional SEM images show that continuous film layers are formed for all

compositions, with generally dense cross-sections and no obvious voids or through-thickness defects, providing a reliable morphological basis for the subsequent dielectric and high-field energy-storage measurements[24,25]. AFM topography and corresponding amplitude images reveal microscale undulations and textured features on the surfaces of the films across different compositions. Overall, blending does not compromise the macroscopic structural continuity of the films[12].

The dielectric constant and dielectric loss quantify a material's capacity to store electrostatic energy and dissipate it under an applied electric field. Figure 3A and B display the dielectric spectra of P(VDF-TrFE-CFE)/PMMA blend films, illustrating how these properties vary with composition. With increasing frequency, the dielectric constant decreases for all samples. In contrast, the dielectric loss first decreases and then increases, a trend attributed to the inability of dipole reorientation to follow rapid field alterations at higher frequencies[26]. Furthermore, the dielectric constant decreases monotonically with higher PMMA content. This reduction is linked to the amorphous structure of PMMA, where spontaneous dipole alignment is hindered, resulting in low macroscopic electroactivity. When incorporated into the P(VDF-TrFE-CFE) matrix, PMMA can reduce the overall polarization response in two ways[27,28]. First, it dilutes the contribution from the highly polar fluorinated/chlorinated segments. Second, dipolar interactions between PMMA and P(VDF-TrFE-CFE) impose additional intermolecular constraints, which further suppress cooperative dipolar polarization. As a result, the dielectric constant decreases progressively as the PMMA fraction increases, and the corresponding dielectric constants at 10 kHz are summarized in Figure 3C. Regarding dielectric loss [Figure 3B and D], pristine P(VDF-TrFE-CFE) exhibits a noticeably higher loss across the entire frequency range, with a rapid increase at higher frequencies - an evolution commonly observed for relaxor ferroelectric polymers such as P(VDF-TrFE-CFE). With increasing PMMA content in the blend films, the dielectric loss in the high-frequency region is markedly suppressed.

Breakdown strength is a key determinant of the energy storage performance of polymer dielectrics; here, it is statistically assessed using a Weibull analysis of the film breakdown data. The Weibull distribution is expressed as:

$$X_i = \ln(E_i) \tag{1}$$

$$Y_i = \ln(-\ln(1 - i/(n+1))) \tag{2}$$

where n and i are the total number of samples and the sample serial number, respectively, with E_i being the breakdown electric field of each specimen[29]. The shape parameter (β), obtained from the slope of X_i-Y_i linear fit, characterizes the dispersion of the breakdown data, and a high β value indicates greater reliability in the measured E_b. The E_b is defined by the intercept point of the fitted line at $Y_i = 0$. Figure 4A shows the Weibull statistical analysis of the breakdown strength for P(VDF-TrFE-CFE)/PMMA blend films with different PMMA contents. The overall linear fitting is satisfactory, indicating good reliability of the breakdown behavior. The corresponding characteristic breakdown strengths are summarized in Figure 4B. Introducing PMMA markedly enhances the breakdown strength, which increases from 5,120 kV/cm for pristine P(VDF-TrFE-CFE) to 7,500 kV/cm for the 70/30 wt.% blend. The representative unipolar *P-E* loops and corresponding energy-storage performance of the optimized P(VDF-TrFE-CFE)/PMMA 50/50 wt.% film are shown in Figure 4C, where a discharged energy density of 17.12 J/cm^3 and an energy-storage efficiency of 88.11% are achieved while maintaining a high breakdown strength of 6,941 kV/cm. For comparison, the representative *P-E* loops of the other compositions are provided in Supplementary Figure 5. The enhanced electrical performance likely arises from several factors. PMMA itself is a linear polymer with high dielectric strength, which helps improve the electrical robustness of the blends. In addition, dipole-dipole interactions between the PMMA carbonyl groups and the polar groups in P(VDF-TrFE-CFE),

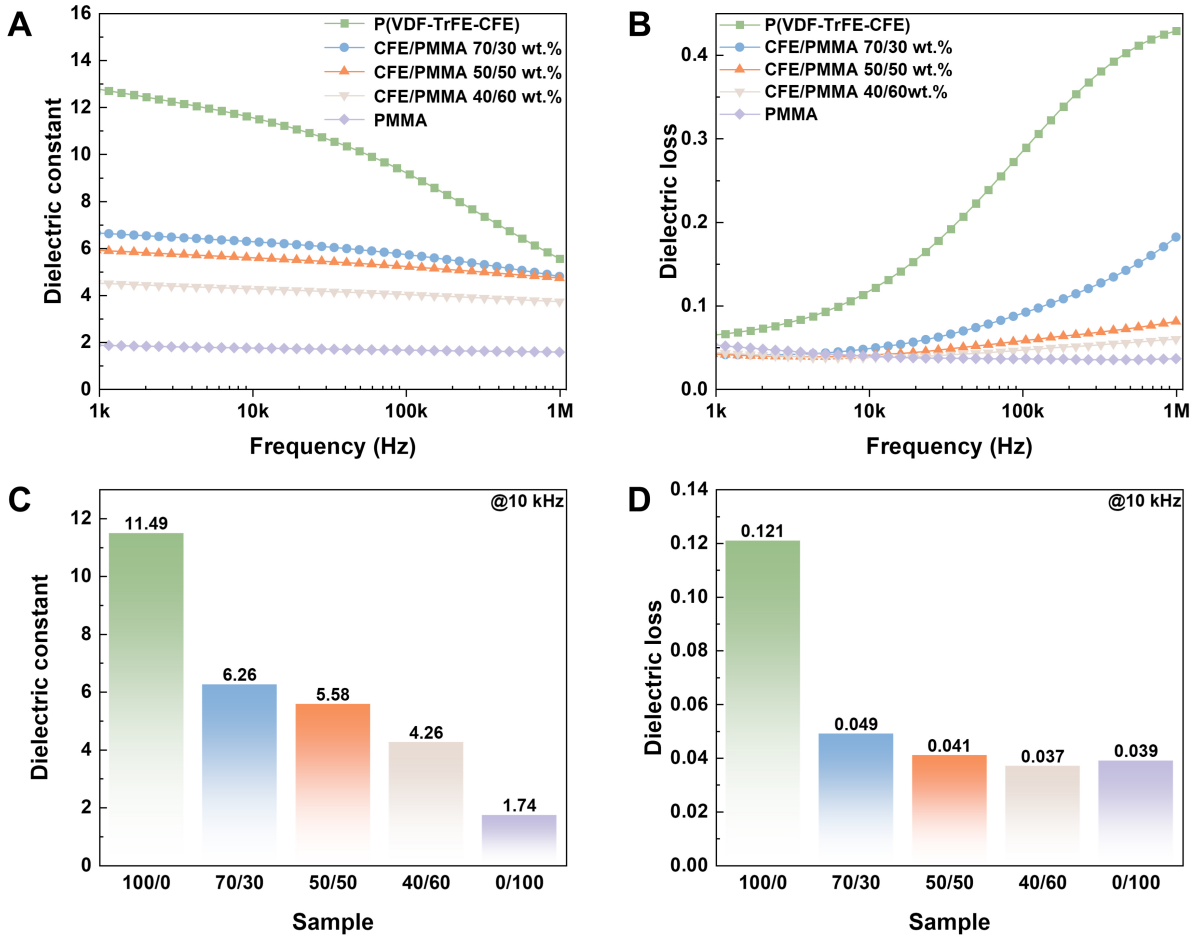

Figure 3. Dielectric spectral characteristics of P(VDF-TrFE-CFE)/PMMA blend films. (A) Frequency-dependent dielectric constant; (B) frequency-dependent dielectric loss; (C) dielectric constant at 10 kHz; (D) dielectric loss at 10 kHz. P(VDF-TrFE-CFE): Poly(vinylidene fluoride- trifluoroethylene-chlorofluoroethylene); PMMA: poly(methyl methacrylate); CFE: abbreviation of P(VDF-TrFE-CFE).

together with altered chain packing and suppressed crystallization, may promote segmental confinement and hinder carrier transport[30-34]. As an amorphous component, PMMA also disrupts the more continuous crystalline regions of P(VDF-TrFE-CFE), thereby blocking carrier-transport pathways and contributing to the increased breakdown strength[34]. From the perspective of conduction behavior, enhanced breakdown strength is often accompanied by suppressed leakage current. Accordingly, the leakage current density and volume resistivity of the films are further measured under different electric fields [Supplementary Figure 6]. Compared with pristine P(VDF-TrFE-CFE), the PMMA-containing blends exhibit overall lower leakage current densities while maintaining higher resistivity, which is consistent with the view that the amorphous insulating PMMA matrix and the blend-specific heterointeractions help suppress carrier injection and transport. However, when the PMMA content is further increased, the breakdown strength of the blend films shows a slight decrease. This behavior may be related to excessive disruption of the residual ordered regions of P(VDF-TrFE-CFE) and the formation of local structural defects during thermal treatment, which could limit further improvement in breakdown strength.

Meanwhile, the maximum polarization (P_{max}) and remanent polarization (P_r) were evaluated, and the polarization difference (P_{max}-P_r) is used to represent the releasable polarization response during the charge-discharge cycle. As shown in Figure 4D, based on the *P*-*E* loops in Figure 4C and Supplementary Figure 5, although the P_{max} of some samples decreases compared with pristine P(VDF-TrFE-CFE) due to the incorporation of a large fraction of low-electroactivity PMMA, the P_r is also markedly suppressed. The

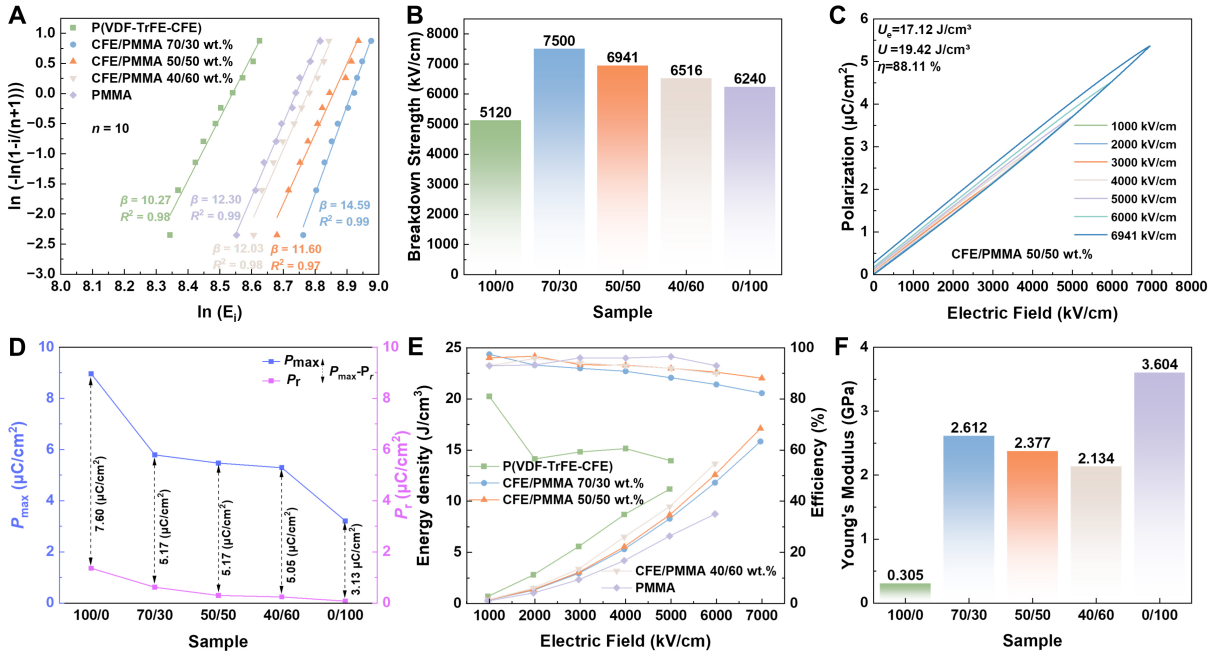

Figure 4. Breakdown statistics and energy-storage performance of P(VDF-TrFE-CFE)/PMMA blend films. (A) Weibull distribution of breakdown strength for films with different compositions; (B) characteristic breakdown strength E_b obtained from Weibull fitting; (C) unipolar *P-E* loops of the P(VDF-TrFE-CFE)/PMMA 50/50 wt.% film under different applied electric fields and the corresponding energy-storage parameters (U_e, U, η); (D) maximum polarization P_{max}, remanent polarization P_r, and polarization difference for films with different compositions; (E) electric-field-dependent discharged energy density and energy-storage efficiency for films with different compositions; (F) Young's modulus of films with different compositions. *P-E*: Polarization-electric field; P(VDF-TrFE-CFE): poly(vinylidene fluoride-trifluoroethylene-chlorofluoroethylene); PMMA: poly(methyl methacrylate); CFE: abbreviation of P(VDF-TrFE-CFE); P_{max}: maximum polarization; P_r: remanent polarization; U_e: discharged energy density; U: total energy density; η: energy-storage efficiency.

resulting composition-dependent energy-storage performance is summarized in Figure 4E. Mechanical robustness can also influence the breakdown strength of the blend films. Figure 4F presents the Young's modulus of films with different compositions. Pristine P(VDF-TrFE-CFE) exhibits a relatively low modulus of only 0.305 GPa, whereas the modulus increases markedly after incorporating PMMA and becomes significantly higher than that of pristine P(VDF-TrFE-CFE). Specifically, among the blend compositions, the modulus reaches 2.612 GPa for the 70/30 blend and then decreases to 2.377 and 2.134 GPa for the 50/50 and 40/60 blends, respectively, indicating a non-monotonic composition dependence. This behavior likely reflects a balance between the rigidifying contribution of PMMA and the progressive disruption of the residual ordered packing of P(VDF-TrFE-CFE) with increasing PMMA content. Accordingly, the 70/30 film appears to retain sufficient terpolymer-related structural continuity while already benefiting from the rigid PMMA component, giving the highest modulus among the blend films. With further increasing PMMA content, the increasingly amorphous blend structure offsets the stiffening effect of PMMA, leading to a decrease in modulus. Neat PMMA exhibits the highest modulus overall because it is a single rigid amorphous polymer, whereas the blend films are mechanically coupled two-component systems. Therefore, the enhanced breakdown strength cannot be attributed to mechanical stiffness alone, but should be understood as the combined result of mechanical robustness, crystallization suppression, reduced carrier transport, and improved structural homogeneity[35].

Beyond high energy-storage capability, the stability and reliability of dielectrics are also critical performance metrics. Therefore, the P(VDF-TrFE-CFE)/PMMA 50/50 wt.% blend film, which exhibits the best overall performance, is selected to evaluate frequency stability and fatigue cycling stability at 3,000 kV/cm, and the results are summarized in Figure 5. The unipolar *P-E* loops measured at different frequencies from 50 Hz to

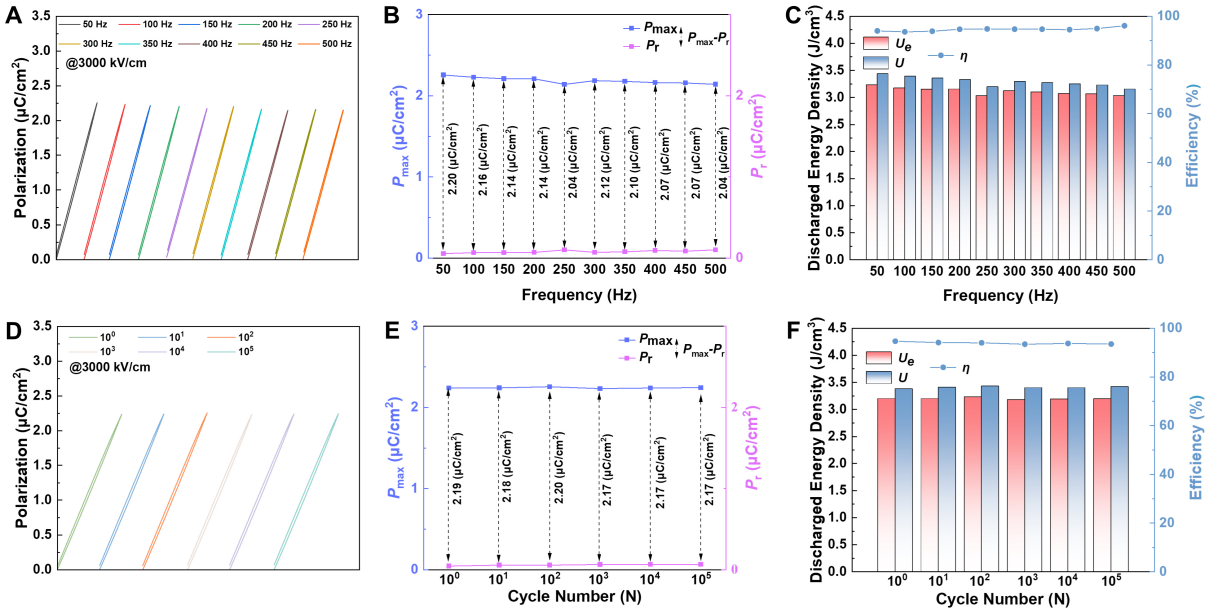

Figure 5. Frequency and cycling stability of the P(VDF-TrFE-CFE)/PMMA 50/50 wt.% film measured at 3,000 kV/cm. (A) Unipolar *P-E* loops measured at different frequencies (50-500 Hz); (B) P_{max}, P_r, and polarization difference at different frequencies; (C) discharged energy density U_e, total energy density U, and energy efficiency η at different frequencies; (D) Unipolar *P-E* loops after different cycle numbers; (E) P_{max}, P_r, and polarization difference versus cycle number; (F) U_e, U, and η versus cycle number. *P-E*: Polarization-electric field; P(VDF-TrFE-CFE): poly(vinylidene fluoride-trifluoroethylene-chlorofluoroethylene); PMMA: poly(methyl methacrylate); CFE: abbreviation of P(VDF-TrFE-CFE); P_{max}: maximum polarization; P_r: remanent polarization; U_e: discharged energy density; U: total energy density; η: energy-storage efficiency.

500 Hz are shown in Figure 5A, and the corresponding polarization parameters (P_{max}, P_r, and P_{max}-P_r) are summarized in Figure 5B. The discharged energy density, total energy density, and energy-storage efficiency are further compared in Figure 5C. Likewise, the fatigue-cycling behavior from 10^0 to 10^5 cycles is presented by the unipolar *P-E* loops in Figure 5D, with the corresponding polarization parameters summarized in Figure 5E and the related energy-storage performance shown in Figure 5F. Within the frequency range of 50-500 Hz and over 10^0-10^5 cycles, the unipolar *P-E* loops remain consistently slim. Across the tested frequency and cycling windows, the variations in U_e and η are only 6.2% and 2.5%, and 1.2% and 0.9%, respectively, indicating excellent frequency and cycling-reliability of the capacitive performance.

To further explore the energy-storage potential of this system, the P(VDF-TrFE-CFE)/PMMA 50/50 wt.% film with the best overall performance was subjected to γ-irradiation at different doses (10-150 kGy), and its structural and electrical responses are comparatively analyzed [Figure 6, Supplementary Figures 7 and 8]. From a structural perspective, the irradiated films remain dominated by a broad diffuse halo in the XRD patterns [Figure 6A]. No new crystalline diffraction peaks are observed after γ-irradiation. These results suggest that γ-irradiation does not induce the formation of a new crystalline phase and that the films still retain an amorphous-dominant structural feature. To further quantify the XRD evolution, the peak position of the broad diffraction feature is tracked as a function of irradiation dose [Supplementary Figure 9]. The feature gradually shifts from 16.25° to 21.00°, corresponding to a decrease in the calculated d-spacing from 5.45 Å to 4.23 Å. This result suggests that γ-irradiation affects the average spacing or local packing associated with this broad diffraction feature. Meanwhile, the FTIR spectra show a dose-dependent enhancement in the carbonyl-related absorption [Figure 6B], suggesting that oxidation-associated structural evolution is an important consequence of γ-irradiation in the present films[36]. It should be noted, however, that the irradiation effect is unlikely to be limited to carbonyl formation alone. Based on previous reports on irradiated P(VDF-TrFE) polymers, γ-irradiation may also induce concurrent structural changes, including

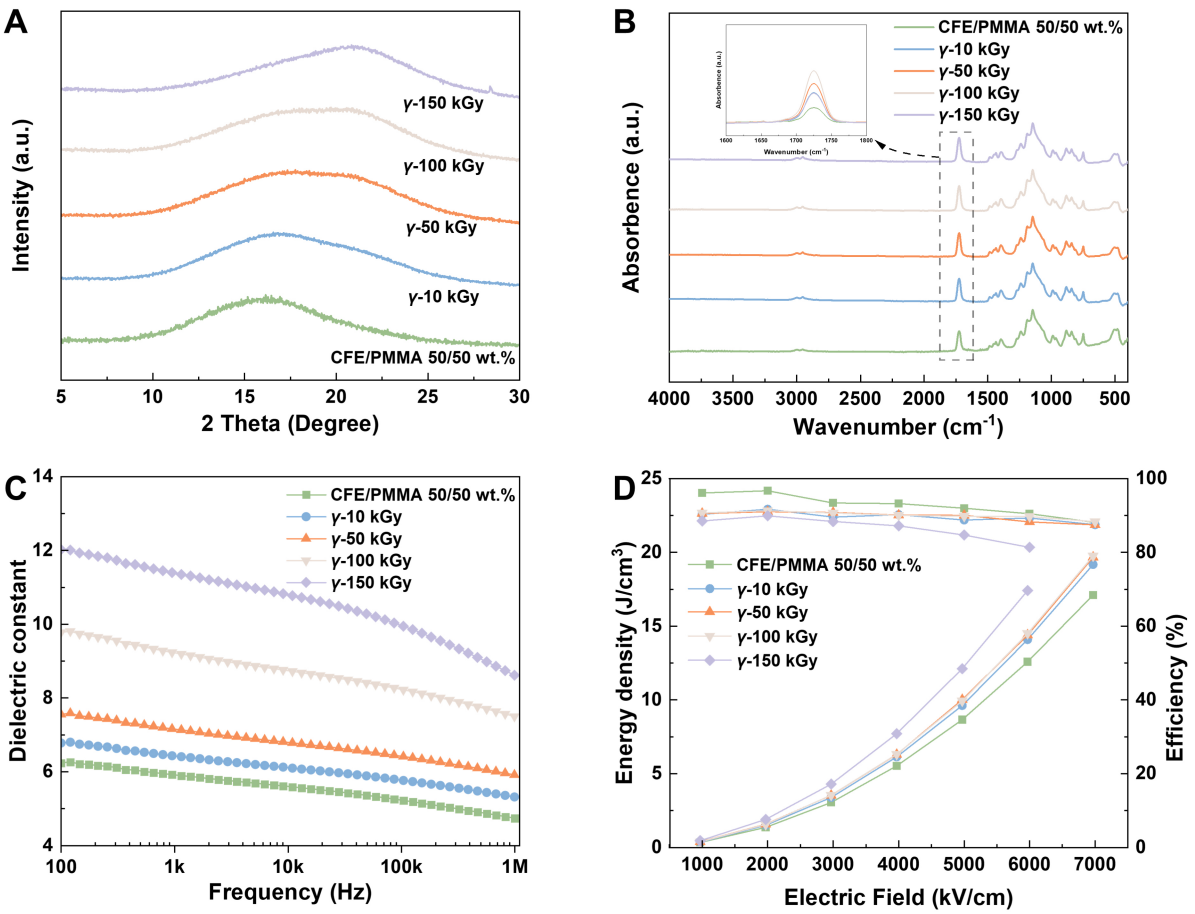

Figure 6. Effects of γ-irradiation on the structure and electrical responses of the P(VDF-TrFE-CFE)/PMMA (50/50 wt.%) film. (A) XRD patterns of the films irradiated at different doses (10, 50, 100, and 150 kGy); (B) FTIR spectra with a zoom-in view of the carbonyl region, showing more pronounced carbonyl-related spectral changes with increasing dose; (C) frequency-dependent dielectric constant of the irradiated films; (D) energy density and efficiency of the irradiated films measured under different electric fields. XRD: X-ray diffraction; FTIR: fourier transform infrared; P(VDF-TrFE-CFE): poly(vinylidene fluoride-trifluoroethylene-chlorofluoroethylene); PMMA: poly(methyl methacrylate); CFE: abbreviation of P(VDF-TrFE-CFE).

unsaturated structures, crosslinking in amorphous regions, and disordering or size reduction of crystalline regions. Such combined structural evolution may enhance dielectric performance through two main effects. First, the generation of additional polar oxygen-containing groups can strengthen dipolar polarization and increase the dielectric permittivity. Second, irradiation-induced disorder and constrained carrier transport can weaken ferroelectric long-range ordering, suppress remanent polarization and hysteresis loss, and reduce electrical dissipation, which helps maintain high energy-storage efficiency[37,38]. In terms of electrical performance, at an irradiation dose of 100 kGy, the dielectric constant at 10 kHz increases from 5.58 to 8.75 [Figure 6C]. Meanwhile, a higher discharged energy density of ~28.14 J/cm³ is achieved, representing a 64.37% improvement over the untreated sample, while a high energy-storage efficiency of ~87.44% is still maintained [Figure 6D and Supplementary Figure 8]. These results indicate that 100 kGy provides the best balance between enhanced polarization response and reduced electrical loss, thereby leading to the optimal overall energy storage performance.

As shown in Supplementary Figure 10, the discharged energy density and efficiency achieved in this work are benchmarked against representative PVDF-based ferroelectric polymer systems reported in recent years[12,13,18,21,39-44]. Many previously reported blend or composite strategies improve either energy density or efficiency, but achieving both simultaneously remains challenging. In particular, the incorporation of linear

polymer components is often effective in enhancing breakdown strength and suppressing dielectric loss, whereas the corresponding reduction in dielectric constant and polarization response may limit the increase in discharged energy density. By contrast, ferroelectric-rich systems usually provide higher polarization but are often accompanied by larger hysteresis loss and lower efficiency. Compared with these representative systems, the P(VDF-TrFE-CFE)/PMMA blend developed in this work exhibits a more favorable balance between discharged energy density and efficiency. In particular, the optimized composition delivers high energy-storage performance while maintaining a relatively high efficiency, underscoring the effectiveness of all-organic blend design in regulating intermolecular interactions, crystallization behavior, and microstructure. These results demonstrate that the present strategy provides an effective route for developing high-performance polymer dielectrics for advanced capacitive energy-storage applications.

CONCLUSIONS

In this work, all-organic P(VDF-TrFE-CFE)/PMMA blend films were designed and fabricated to improve the energy-storage performance of polymer dielectrics through composition regulation and γ-irradiation treatment. The introduction of PMMA effectively modified the microstructure and electrical behavior of P(VDF-TrFE-CFE), leading to suppressed crystallization, enhanced breakdown strength, and improved energy-storage performance. Among the unirradiated blend films, the 50/50 wt.% composition exhibited the best overall performance, delivering a discharged energy density of 17.12 J/cm^3 with an efficiency of 88.11%. Further γ-irradiation of this optimized blend film provided an additional performance enhancement, and the 100 kGy sample achieved a discharged energy density of 28.14 J/cm^3 while maintaining a high efficiency of 87.44%. These results demonstrate that the combination of all-organic blending and irradiation engineering provides an effective strategy for developing high-performance polymer dielectric materials for advanced energy-storage applications.

DECLARATIONS

Authors' contributions

Methodology, formal analysis, and writing of the manuscript: Wu, Y.; Zhang, Z.; Zhang, Y.; Ma, Z.
Data analysis and technical support: Bai. B.; Liu, W.
Data acquisition: Deng, C.; Zhang, S.
Analysis and interpretation of the results: Wu, Y.; Zhang, Z.
Supervision, writing - review and editing: Huang, Y.; Zhang, Q.; Hu, Y.
All authors discussed the results and commented on the manuscript.

Availability of data and materials

Some results of supporting the study are presented in the Supplementary Materials. Other raw data that supports the findings of this study are available from the corresponding author upon reasonable request.

AI and AI-assisted tools Statement

Not applicable.

Financial support and sponsorship

This research was supported by the National Natural Science Foundation of China (Grant No. U24A20203, 52572127, 52172113), Shenzhen Science and Technology Program (Grant No. RCBS20231211090700002), and Science and Technology Innovation Base of Hubei Province (Platform) (Grant No. 2025CSA063, 2025CSA140).

Conflicts of interest

All authors declared that there are no conflicts of interest.

Ethical approval and consent to participate

Not applicable.

Consent for publication

Not applicable.

Supplementary Materials

Supplementary Materials

REFERENCES

1. Yang, Z.; Yue, D.; Yao, Y.; et al. Energy storage application of all-organic polymer dielectrics: a review. *Polymers* **2022**, *14*, 1160. DOI PubMed PMC
2. Luo, H.; Wang, F.; Guo, R.; et al. Progress on polymer dielectrics for electrostatic capacitors application. *Adv. Sci.* **2022**, *9*, 2202438. DOI PubMed PMC
3. Yang, D.; Gao, J.; Shu, L.; et al. Lead-free antiferroelectric niobates $AgNbO_3$ and $NaNbO_3$ for energy storage applications. *J. Mater. Chem. A.* **2020**, *8*, 23724-37. DOI
4. Liu, Y.; Luo, H.; Chen, H.; et al. Gradient structured all-organic dielectrics by electrospinning for enhanced energy storage performance. *J. Mater. Chem. A.* **2024**, *12*, 12501-14. DOI
5. Yang, M.; Li, H.; Wang, J.; et al. Roll-to-roll fabricated polymer composites filled with subnanosheets exhibiting high energy density and cyclic stability at 200 °C. *Nat. Energy.* **2024**, *9*, 143-53. DOI
6. Wang, J.; Guo, H.; Zeng, S.; Du, J.; Zhang, Q.; Wang, K. Thin, largescale processed, high-temperature resistant capacitor films based on polypropylene/cycloolefin copolymer blend. *Chem. Eng. J.* **2024**, *492*, 152237. DOI
7. Dan, Z.; Jiang, J.; Qian, J.; et al. A Ferroconcrete-like all-organic nanocomposite exhibiting improved mechanical property, high breakdown strength, and high energy efficiency. *Macromol. Mater. Eng.* **2019**, *304*, 1900433. DOI
8. Chu, B.; Zhou, X.; Ren, K.; et al. A Dielectric polymer with high electric energy density and fast discharge speed. *Science* **2006**, *313*, 334-6. DOI
9. Huang, Y.; Xu, J.; Soulestin, T.; et al. Can relaxor ferroelectric behavior be realized for poly(vinylidene fluoride-*co*-chlorotrifluoroethylene) [P(VDF-CTFE)] random copolymers by inclusion of CTFE units in PVDF crystals? *Macromolecules* **2018**, *51*, 5460-72. DOI
10. Ren, X.; Meng, N.; Zhang, H.; et al. Giant energy storage density in PVDF with internal stress engineered polar nanostructures. *Nano. Energy.* **2020**, *72*, 104662. DOI
11. Furukawa, T.; Date, M.; Fukada, E. Hysteresis phenomena in polyvinylidene fluoride under high electric field. *J. Appl. Phys.* **1980**, *51*, 1135-41. DOI
12. Zhang, Y.; Huang, S.; Tan, H.; et al. Ultra-high energy density in all-organic copolymeric blends by grain refinement. *J. Mater. Chem. C.* **2025**, *13*, 16242-51. DOI
13. Zhang, C.; Zhang, T.; Feng, M.; et al. Significantly improved energy storage performance of PVDF ferroelectric films by blending PMMA and filling PCBM. *ACS. Sustainable. Chem. Eng.* **2021**, *9*, 16291-303. DOI
14. Han, Y.; Shen, M.; Xu, Y.; Yang, L.; Xue, Y.; Tao, W. Synchronously promoted discharged energy density and discharged efficiency in PVDF films through a linear dielectric polymer PP blending approach. *J. Mater. Sci. Mater. Electron.* **2021**, *32*, 6249-59. DOI
15. Luo, B.; Wang, X.; Wang, H.; Cai, Z.; Li, L. P(VDF-HFP)/PMMA flexible composite films with enhanced energy storage density and efficiency. *Compos. Sci. Technol.* **2017**, *151*, 94-103. DOI
16. Chi, Q.; Zhou, Y.; Yin, C.; et al. A blended binary composite of poly(vinylidene fluoride) and poly(methyl methacrylate) exhibiting excellent energy storage performances. *J. Mater. Chem. C.* **2019**, *7*, 14148-58. DOI
17. Wang, C.; He, G.; Chen, S.; Luo, H.; Yang, Y.; Zhang, D. Achieving high breakdown strength and energy density in all-organic sandwich-structured dielectrics by introducing polyacrylate elastomers. *J. Mater. Chem. A.* **2022**, *10*, 9103-13. DOI
18. Zheng, S.; Xie, J.; Zhao, X.; Sun, S. Methyl methacrylate-co-glycidyl methacrylate-based dielectric films with high breakdown strength and discharge energy density tailored by PVDF. *Langmuir* **2023**, *39*, 3710-9. DOI
19. Bao, H.; Song, J.; Zhang, J.; Shen, Q.; Yang, C.; Zhang, Q. M. Phase transitions and ferroelectric relaxor behavior in P(VDF-TrFE-CFE) terpolymers. *Macromolecules* **2007**, *40*, 2371-9. DOI
20. Li, F.; Wang, L.; Gao, L.; et al. Reducing dielectric loss of high-dielectric-constant elastomer via rigid short-chain crosslinking. *Adv. Mater.* **2024**, *36*, 2411082. DOI
21. Liu, C.; Li, D.; Wang, Z.; et al. Massively parallel aligned poly(vinylidene fluoride) nanofibrils in all-organic dielectric polymer composite films for electric energy storage. *Macromolecules* **2023**, *56*, 1481-91. DOI

22. Cheng, Y.; Ji, Q.; Zhang, G.; et al. Synergistic Enhancement of dielectric polymers through fluorine incorporation for improved energy storage, reduced loss, and enhanced processability. *Adv. Funct. Mater.* **2024**, *34*, 2406219. DOI
23. Yu, X.; Li, L.; Gao, J.; et al. Ultra-high energy density in cyanoethyl biomass polymers. *Adv. Funct. Mater.* **2024**, *34*, 2404613. DOI
24. Li, Y.; Soulestin, T.; Ladmiral, V.; et al. Stretching-induced relaxor ferroelectric behavior in a poly(vinylidene fluoride-*co*-trifluoroethylene-*co*-hexafluoropropylene) random terpolymer. *Macromolecules* **2017**, *50*, 7646-56. DOI
25. Liu, K.; Liu, Y.; Ma, W.; et al. Realizing enhanced energy density in ternary polymer blends by intermolecular structure design. *Chem. Eng. J.* **2022**, *446*, 136980. DOI
26. Zhang, J.; Du, X.; Wang, C.; Ren, K. Poly(vinylidene fluoride-hexafluoropropylene) based blend film for ultrahigh energy density capacitor applications. *J. Phys. D. Appl. Phys.* **2018**, *51*, 255306. DOI
27. Li, H.; Zhou, Y.; Liu, Y.; Li, L.; Liu, Y.; Wang, Q. Dielectric polymers for high-temperature capacitive energy storage. *Chem. Soc. Rev.* **2021**, *50*, 6369-400. DOI
28. Dong, X.; Wan, B.; Zha, J. Versatile landscape of Low-*k* polyimide: theories, synthesis, synergistic properties, and industrial integration. *Chem. Rev.* **2024**, *124*, 7674-711. DOI
29. Melianas, A.; Felekidis, N.; Puttisong, Y.; et al. Nonequilibrium site distribution governs charge-transfer electroluminescence at disordered organic heterointerfaces. *Proc. Natl. Acad. Sci. U.S.A.* **2019**, *116*, 23416-25. DOI PubMed PMC
30. Fan, Y.; Iwashita, T.; Egami, T. Energy landscape-driven non-equilibrium evolution of inherent structure in disordered material. *Nat. Commun.* **2017**, *8*, 15417. DOI PubMed PMC
31. Fediai, A.; Symalla, F.; Friederich, P.; Wenzel, W. Disorder compensation controls doping efficiency in organic semiconductors. *Nat. Commun.* **2019**, *10*, 4547. DOI PubMed PMC
32. Li, J.; Shen, Z.; Chen, X.; et al. Grain-orientation-engineered multilayer ceramic capacitors for energy storage applications. *Nat. Mater.* **2020**, *19*, 999-1005. DOI
33. Zeng, T.; Meng, L.; Li, Q.; et al. Enhancing energetic disorder in all-organic composite dielectrics for high-temperature capacitive energy storage. *Nat. Commun.* **2025**, *16*, 5620. DOI PubMed PMC
34. Wang, T.; Zhang, M.; Song, R.; et al. Ultrahigh energy density in all-organic composites synergistically tailored by PMMA and molecular semiconductor. *Adv. Funct. Mater.* **2025**, *35*, 2422652. DOI
35. Zhao, X.; Zhang, L.; Fan, Z.; et al. Excellent high-temperature dielectric energy storage performance in bilayer nanocomposites with high-entropy ferroelectric oxide fillers. *Nat. Commun.* **2025**, *16*, 5570. DOI PubMed PMC
36. Wang, Y.; Bao, Z.; Ding, S.; et al. γ-ray irradiation significantly enhances capacitive energy storage performance of polymer dielectric films. *Adv. Mater.* **2024**, *36*, 2308597. DOI
37. Tang, Y.; Wang, D.; Guo, S.; Zhao, X. Effect of γ-ray radiation on structure of P(VDF/TrFE) 80/20 mol% copolymers. *Eur. Polym. J.* **2001**, *37*, 471-4. DOI
38. Shim, H.; Lee, B.; Lim, D.; Nam, Y.; Choi, P.; Gwon, H. A comparative study of gamma-ray irradiation-induced oxidation: polyethylene, poly(vinylidene fluoride), and polytetrafluoroethylene. *Polymers* **2022**, *14*, 4570. DOI
39. Sun, S.; Shi, Z.; Sun, L.; et al. Achieving concurrent high energy density and efficiency in all-polymer layered paraelectric/ferroelectric composites via introducing a moderate layer. *ACS. Appl. Mater. Interfaces.* **2021**, *13*, 27522-32. DOI
40. Yang, L.; Liu, X.; Lu, Z.; et al. Optimizing nanostructures to achieve enhanced breakdown strength and improved energy storage performances in dipolar polymers. *Nanoscale* **2022**, *14*, 14135-45. DOI
41. Zhang, C.; Tong, X.; Liu, Z.; et al. Enhancement of energy storage performance of PMMA/PVDF composites by changing the crystalline phase through heat treatment. *Polymers* **2023**, *15*, 2486. DOI PubMed PMC
42. Zhu, T.; Zhao, H.; Zhang, N.; et al. Ultrahigh energy storage density in poly(vinylidene fluoride)-based composite dielectrics via constructing the electric potential well. *Adv. Energy. Mater.* **2023**, *13*, 2203587. DOI
43. Zhu, H.; Liu, X.; Bai, H.; Yang, T. Antiferroelectric nano-heterostructures filler for improving energy storage performance of PVDF-based composite films. *Chem. Eng. J.* **2024**, *479*, 147572. DOI
44. Sun, X.; Zheng, Y.; Liu, K.; et al. Gradient core-shell structure enabling high energy storage performances in PVDF-based copolymers. *J. Mater. Chem. A.* **2024**, *12*, 8216-25. DOI